Electrochemistry

DOI: 10.1002/anie.200903587

$LiMn_{0.8}Fe_{0.2}PO_4$: An Advanced Cathode Material for Rechargeable Lithium Batteries**

*Surendra K. Martha, Judith Grinblat, Ortal Haik, Ella Zinigrad, Thierry Drezen, James H. Miners, Ivan Exnar, Andreas Kay, Boris Markovsky, and Doron Aurbach**

Since the pioneering studies of Goodenough and co-workers,[1] $LiMPO_4$ compounds (M = Fe, Mn, Co, or Ni, theoretical capacity around 170 $mA\,h\,g^{-1}$) have been investigated as promising cathode materials for rechargeable lithium-ion batteries.[2] $LiFePO_4$ is now recognized as one of the most promising cathode materials owing to the existence of a variety of synthetic routes for its production as nanoparticles coated with conducting phases (e.g. carbon).[3] The inherent low cost, nontoxicity, and extremely high stability of $LiFePO_4$ has naturally led to intensive battery development toward large-scale applications, such as plug-in hybrid vehicles.[4] This material has intrinsically poor ionic and electronic conductivity.[5] However, when nanoparticles were used as the active mass and coated with thin, electronically conductive layers, impressive rate capabilities were demonstrated with $LiFePO_4$ cathodes in practical lithium-ion batteries.[6,7]

$LiMnPO_4$ is a much more promising cathode material for lithium-ion batteries than $LiFePO_4$ as a result of its higher redox voltage of 4.2 V ($LiFePO_4$: 3.5 V) versus Li/Li^+. We demonstrated recently[8] that carbon-coated nanoparticles of $LiMnPO_4$ can indeed be used as a practical cathode material with a capacity of around 145 $mA\,h\,g^{-1}$, acceptable rate capabilities, and impressive stability. $LiMnPO_4$ cathodes can be cycled many hundreds of times even at elevated temperatures (e.g. 60 °C) with relatively low capacity fading. However, since the specific capacity and rate capability of this material were lower than those of $Li(MnNiCo)O_2$ (layered) cathode materials, there is a strong incentive to increase the rate capability of $LiMnPO_4$. Once this rate-capacity problem is solved, it will be possible to utilize $LiMnPO_4$ in advanced lithium-ion batteries owing to its unique advantages: high and flat voltage as well as excellent stability and safety features in standard electrolyte solutions. Previous reports on $Li(MnFe)PO_4$ compounds suggest that such mixed-transition-metal olivine compounds may have a higher rate capability than $LiMnPO_4$; however, it is not clear what the optimal ratio of Mn and Fe in these compounds may be or to what extent these compounds are stable as cathodes for lithium batteries.[1,9,10] Since the redox potential of the Fe ions in the olivine compounds is lower by 600–700 mV than that of Mn ions, it is important to maximize the Mn/Fe ratio in $Li(MnFe)PO_4$ to ensure that most of the capacity is available in the high-voltage domain.

We report herein on carbon-coated nanoparticles of $LiMn_{0.8}Fe_{0.2}PO_4$ (C–$LiMn_{0.8}Fe_{0.2}PO_4$) as a superb cathode material for advanced lithium-ion batteries. We found that the replacement of 20% of the Mn atoms in $LiMnPO_4$ with Fe atoms was optimal. Thus, the high redox potential of $LiMnPO_4$ was decreased to a certain extent, which led to improved capacity and a highly impressive rate capability. Electrochemical techniques were used in conjunction with XRD, high-resolution microscopy, and a variety of spectroscopic tools to characterize the new material. $LiPF_6$ (1M) in ethylene carbonate (EC)–dimethyl carbonate (DMC; 1:1) was used for the electrochemical and thermal measurements and can be considered as the standard electrolyte solution. For aging tests, solutions of $LiPF_6$ (1.5M) in EC–DMC (1:2) were used (see the explanation in the Supporting Information).

Carbon-coated nanoparticles of $LiMn_{0.8}Fe_{0.2}PO_4$ were prepared by solid-state synthesis as described in the Experimental Section. Elemental (CHN) analysis showed that the material contained about 10 wt% of carbon. The specific surface of the nanoparticles, as measured by N_2 absorption on the basis of the Brunauer, Emmett, and Teller (BET) model, was 65 $m^2\,g^{-1}$, with the following particle-size distribution: $d(0.1) = 1.5\ \mu m$, $d(0.5) = 7.3\ \mu m$, $d(0.9) = 26.7\ \mu m$, $d(0.99) = 56\ \mu m$.

Figure 1 presents the X-ray diffraction (XRD) patterns of the C–$LiMn_{0.8}Fe_{0.2}PO_4$ nanomaterial, C–$LiMnPO_4$ nanoparticles (prepared for this study as reported in Ref. [8]), and commercial $LiFePO_4$ (Süd-Chemie Inc.). The lattice parameters calculated from this data are also listed in Figure 1. It is clear that all three materials are pure ordered olivine compounds with an orthorhombic structure (space group *Pnma*). We also concluded that the material

[*] Dr. S. K. Martha, Dr. J. Grinblat, O. Haik, Dr. E. Zinigrad, Dr. B. Markovsky, Prof. D. Aurbach
Department of Chemistry, Bar-Ilan University
Ramat-Gan 52900 (Israel)
Fax: (+972) 3-738-4053
E-mail: aurbach@mail.biu.ac.il
Homepage: http://www.ch.biu.ac.il/people/aurbach
Dr. T. Drezen, Dr. J. H. Miners, Dr. I. Exnar
High Power Lithium (HPL SA), PSE-B, EPFL
1015 Lausanne (Switzerland)
Dr. A. Kay
Laboratory for Photonics and Interfaces
Swiss Federal Institute of Technology, EPFL
1015 Lausanne (Switzerland)

[**] We acknowledge Prof. I. Felner from Racah Institute of Physics, The Hebrew University of Jerusalem for Mössbauer spectroscopy measurements, Dr. L. Zeiri from Ben-Gurion University of the Negev, Beer-Sheva for Raman spectroscopy measurements, and Dr. Yossi Gofer and Dr. Pessia Sharon from Bar Ilan University for the XPS and ICP measurements, respectively. Partial support for this research was obtained from the ISF, Israel Science Foundation.

Supporting information for this article is available on the WWW under http://dx.doi.org/10.1002/anie.200903587.

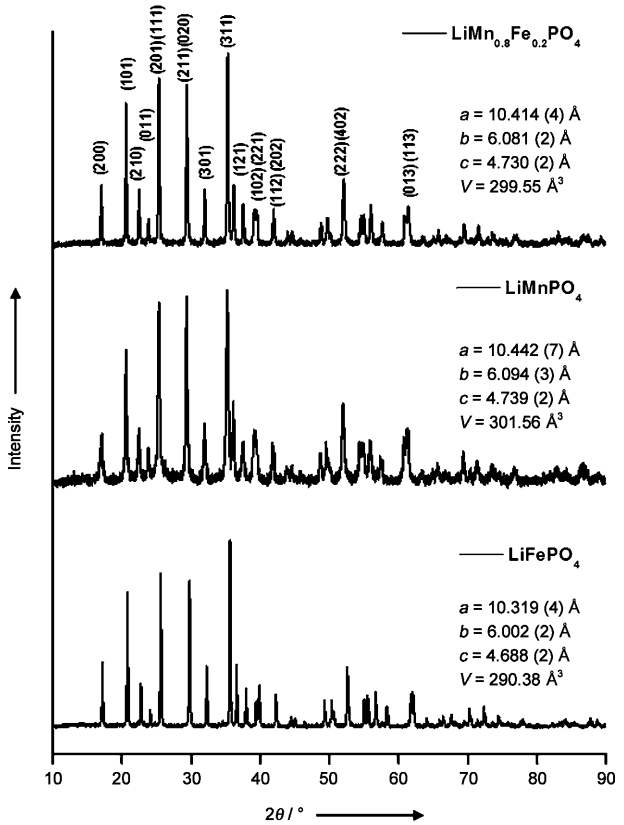

Figure 1. XRD patterns of the C–$LiFePO_4$, C–$LiMnPO_4$, and C–$LiMn_{0.8}Fe_{0.2}PO_4$ particles. Miller indexes of the main reflections and cell parameters are indicated.

C–$LiMn_{0.8}Fe_{0.2}PO_4$ was a solid solution of $LiMnPO_4$ and $LiFePO_4$. Further analysis by Raman spectroscopy (see Figure S1 in the Supporting Information) showed that the $LiMn_{0.8}Fe_{0.2}PO_4$ particles were covered with a highly conductive thin carbon coating. The aging of this material at 60 °C in a solution of $LiPF_6$ (1.5 M) in EC–DMC (1:2) did not substantially change its Raman spectroscopic response. The slight changes (related to the carbon coating) observed in the Raman spectra are in line with the surface studies, which indicated the formation of surface fluorine compounds (including moieties with C–F bonds; see the XPS data in Figure S6 of the Supporting Information).

The morphology of the carbon-coated $LiMn_{0.8}Fe_{0.2}PO_4$ particles was studied by high-resolution transmission electron microscopy (HRTEM) and high-resolution scanning electron microscopy (HRSEM) before and after aging in solutions of $LiPF_6$ (1.5 M) in EC–DMC (1:2) at elevated temperatures. Figure 2 shows HRTEM images of $LiMn_{0.8}Fe_{0.2}PO_4$ particles covered by a 5 nm thick carbon film of 25–60 nm in diameter. The crystallites have a typical, well-defined orthorhombic symmetry, and the atomic layers can also be observed clearly in the image on the right in Figure 2 (see also Figure S2 a in the Supporting Information). High-magnification HRTEM images (see Figure S2 a in the Supporting Information) indicate *d*-spacing values and Miller indices that correspond to the XRD pattern of a material with orthorhombic symmetry. Typical HRTEM images of aged C–$LiMn_{0.8}Fe_{0.2}PO_4$ (3 weeks at 60 °C in a solution of $LiPF_6$ (1.5 M) in EC–DMC (1:2); see Figure S2 b,c in the Supporting Information) showed that the aging of this active mass in the electrolyte solution at elevated temperatures does not change its morphology or structure. The morphology, aging, and stability of the C–$LiMn_{0.8}Fe_{0.2}PO_4$ nanoparticles are further shown by the HRSEM images in Figure S3 a–c of the Supporting Information. Mössbauer spectra of pristine and aged material reflect the response of Fe^{2+} in the compound and further demonstrate the stability of this material upon aging in standard electrolyte solutions at elevated temperatures (see Figure S4 in the Supporting Information).

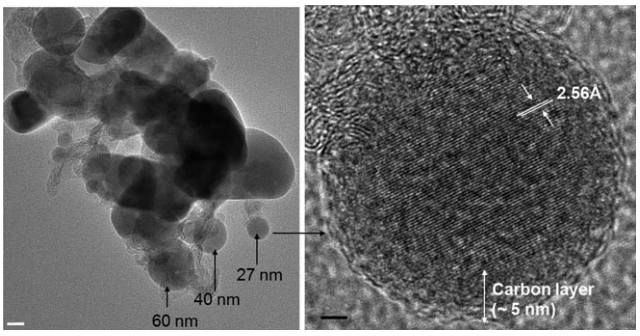

Figure 2. Left: HRTEM image of C–$LiMn_{0.8}Fe_{0.2}PO_4$ particles showing their morphology and particle size (scale bar: 20 nm). Right: HRTEM image of a single C–$LiMn_{0.8}Fe_{0.2}PO_4$ particle showing the thickness of the carbon layer (scale bar: 2 nm) as well as the lattice fringes and atomic layers.

Typical FTIR and XPS spectroscopic studies of pristine and aged particles (several weeks at 60 °C in a solution of $LiPF_6$ (1.5 M) in EC–DMC (1:2); see Figures S5 and S6, respectively, in the Supporting Information) demonstrated further the amazing stability of the C–$LiMn_{0.8}Fe_{0.2}PO_4$ nanoparticles. Their very low surface reactivity stands in contrast to the pronounced surface reactivity of all types of lithiated-transition-metal-oxide cathode materials.[11] FTIR spectra of aged C–$LiMn_{0.8}Fe_{0.2}PO_4$ particles did not show any pronounced changes resulting from aging at 60 °C. The XPS studies showed that the main significant impact of aging is the formation of surface fluorides (mostly LiF and maybe FeF_2; see Figure S6 f, g in the Supporting Information) as well as fluoroorganic compounds (as yet unidentified) as a result of the decomposition of $LiPF_6$ and the unavoidable presence of trace HF in the solutions.[11] The formation of these surface species upon aging explains well the increase in the impedance of C–$LiMn_{0.8}Fe_{0.2}PO_4$ and the slight change in the Raman response upon aging (see Figures S1 and S7 in the Supporting Information). These spectral studies indicated the much lower surface reactivity of the C–$LiMn_{0.8}Fe_{0.2}PO_4$ particles (and other olivine compounds, such as $LiFePO_4$ and $LiMnPO_4$)[7,8] toward alkyl carbonate/$LiPF_6$ solutions than that observed for lithiated-transition-metal-oxide cathode materials, the XPS spectra of which reflect pronounced surface changes after aging experiments. We can attribute the difference in the surface reactivity of lithium–olivine and Li_xMO_y cathode materials to pronounced differences in the nucleophilicity and basicity of their surface oxygen anions;

both properties are much higher for the latter compounds (see the discussion in the Supporting Information). It is logical to assume that the carbon coating of the C–$LiMn_{0.8}Fe_{0.2}PO_4$ particles also contributes to the relatively low surface reactivity of the active mass.

Studies of the dissolution of Li, Mn, and Fe ions and phosphorus compounds derived from C–$LiMn_{0.8}Fe_{0.2}PO_4$ in solutions at elevated temperatures indicate that this material undergoes effective passivation upon aging in solutions (see Figure S8 in the Supporting Information and the related discussion).

Steady-state cyclic voltammetry (CV) of C–$LiMn_{0.8}Fe_{0.2}PO_4$-composite electrodes in the various potential ranges between 2.7 and 4.6 V (25 $\mu V s^{-1}$, solution in $LiPF_6$ (1M)/EC–DMC (1:1) at 30 °C) showed the redox activity of the Mn^{2+}/Mn^{3+} and Fe^{2+}/Fe^{3+} couples (peak potentials at around 4.19/3.95 and 3.6/3.5 V, respectively) at the expected ratio of the charges involved (4:1; Figure 3).

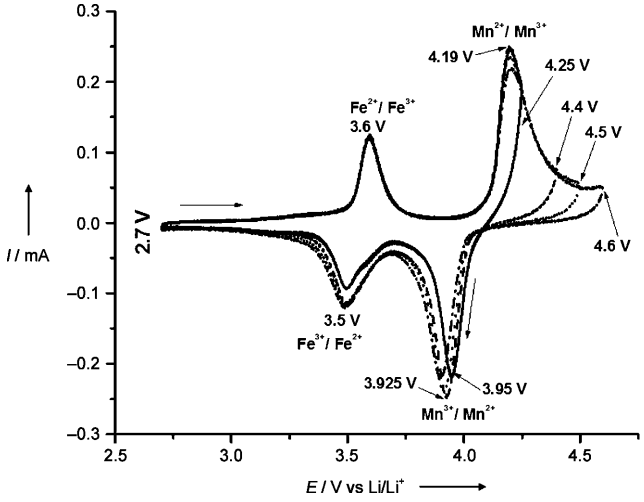

Figure 3. Cyclic voltammograms of C–$LiMn_{0.8}Fe_{0.2}PO_4$ composite electrodes at various cutoff potentials (as indicated) in $LiPF_6$ (1 M)/EC–DMC (1:1) at 30 °C (scan rate: 25 $\mu V s^{-1}$).

Figure S9 in the Supporting Information shows the capacities of the charge and discharge processes (measured by CV) as a function of the maximal (cutoff) charging potential. From these studies, it is clear that the irreversible capacity (i.e. the difference between the charge and discharge capacities) is negligible at cutoff voltages below 4.4 V; thus, reversible capacities of greater than 150 mA h g^{-1} are possible. When higher cutoff voltages were used, reversible capacities higher than 160 mA h g^{-1} could be attained at the expense of increasing the irreversible capacity. The increase in irreversible capacity can be attenuated by the use of surface-reactive additives. For subsequent galvanostatic measurements, it was found that a cutoff potential of 4.25 V was sufficient for reversible capacities of greater than 160 mAh g^{-1} (with zero irreversibility) to be attained.

Typical voltage profiles measured for C–$LiMn_{0.8}Fe_{0.2}PO_4$ electrodes during galvanostatic discharge processes in the standard solution at various rates show the two expected plateaus at around 4.1 and 3.5 V (versus the Li reference electrode) related to the Mn^{2+}/Mn^{3+} and the Fe^{2+}/Fe^{3+} redox couples (Figure 4a). The flat redox-potential response at 4.1 V versus Li/Li^+ clearly indicates a gain of 0.6–0.7 V when

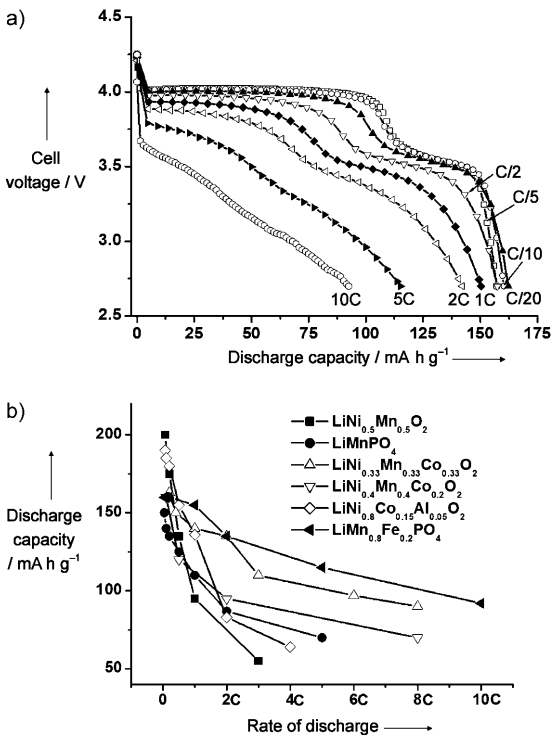

Figure 4. a) Typical voltage profiles of C–$LiMn_{0.8}Fe_{0.2}PO_4$ composite electrodes measured galvanostatically at various discharge rates at 30 °C in the standard electrolyte solution. The term C rate describes the rate of discharge, whereby a constant current is chosen so that the entire maximal specific capacity (165 mA h g^{-1}) is discharged during a specified period of time; for example, the rate C/10 means that the constant current is adjusted to discharge the entire capacity during 10 h, and at rates 1C or 2C the entire capacity is discharged within 1 or 0.5 h, respectively. b) Comparison of rate capabilities (discharge capacity versus discharge rate) for C–$LiMn_{0.8}Fe_{0.2}PO_4$, C–$LiMnPO_4$, $LiNi_{0.33}Mn_{0.33}Co_{0.33}O_2$, $LiNi_{0.4}Mn_{0.4}Co_{0.2}O_2$, $LiNi_{0.5}Mn_{0.5}O_2$, and $LiNi_{0.8}Co_{0.15}Al_{0.05}O_2$ (NCA) cathodes in similar experiments (galvanostatic cycling at 30 °C in standard electrolyte solutions). The potential windows within which C–$LiMn_{0.8}Fe_{0.2}PO_4$, C–$LiMnPO_4$, and the layered transition-metal-oxide cathodes reached their full capacity were 2.7–4.25, 2.7–4.4, and 2.5–4.5 V versus Li/Li^+.

C–$LiMn_{0.8}Fe_{0.2}PO_4$ is compared to $LiFePO_4$. These measurements also demonstrate an impressive rate capability, since at 10C rates (i.e. current densities that correspond to discharge of the entire capacity within 6 min) it was possible to obtain a capacity of approximately 100 mA h g^{-1} from these electrodes. Note that the sloping potential profiles observed at high rates do not relate directly to the cathode, but rather reflect the response of the other resistive components of the cell (anode, solution, and separator) to the high rates.

We compared the rate capabilities of composite electrodes of the following materials: C–$LiMn_{0.8}Fe_{0.2}PO_4$, C–$LiMnPO_4$, $LiNi_{0.33}Mn_{0.33}Co_{0.33}O_2$, $LiNi_{0.4}Mn_{0.4}Co_{0.2}O_2$, $LiNi_{0.5}Mn_{0.5}O_2$, and $LiNi_{0.80}Co_{0.15}Al_{0.05}O_2$ (NCA; Figure 4b). The rate capabilities of the different materials were measured

in identical experiments (with the same ratios between the active mass, carbon additives, and the poly(vinylidene fluoride) (PVdF) binder in the composite electrodes, and the same standard solution and operational protocol; see the Experimental Section). Figure S10 in the Supporting Information shows a similar comparison translated into energy density. Comparison of the rate capability of different electrode materials is not necessarily trivial and straightforward. Also, the specific capacity measured in this study for the electrodes in coin-type cells may be lower than that measured in professional batteries with optimized electrode engineering. However, on a qualitative level, the present comparison should be adequate and meaningful, as further explained in the Supporting Information.

Except for NCA (a commercial product), all materials were prepared by us for this study. The particle size of $LiNi_{0.33}Mn_{0.33}Co_{0.33}O_2$, $LiNi_{0.4}Mn_{0.4}Co_{0.2}O_2$, $LiNi_{0.5}Mn_{0.5}O_2$ (prepared by self-combustion reactions)[12] was submicrometric, optimized for the best stability and rate capability in standard electrolyte solutions.[13] All cathode materials studied were among the most advanced cathode materials in lithium-ion batteries for electric-vehicle (EV) applications. At low rates, the capacity of $Li(MnNi)O_2$ and $Li(NiCoAl)O_2$ is higher than that of C–$LiMn_{0.8}Fe_{0.2}PO_4$ (Figure 4b). However, the rate capability of C–$LiMn_{0.8}Fe_{0.2}PO_4$ is superior, and higher than that of all cathode materials tested. At rates above 2C (i.e. current densities that correspond to discharge of the entire capacity within 30 min), C–$LiMn_{0.8}Fe_{0.2}PO_4$ provided the highest capacities (Figure 4b).

Figure 5 shows typical results of the cycling and stability testing of Li/C–$LiMn_{0.8}Fe_{0.2}PO_4$ cells containing standard electrolyte solutions (see also Figure S11 in the Supporting Information). The rate was changed repeatedly (as indicated in Figure 5) during the prolonged cycling of Li/C–$LiMn_{0.8}Fe_{0.2}PO_4$ cells (30 °C in $LiPF_6$ (1 M)/EC–DMC solutions). In these experiments, a galvanostatic mode was used for discharge, whereas a constant current–constant voltage (CC–CV) protocol was used for charging (see the Experimental Section). The potential limits for these tests were 2.5 and 4.25 V. An initial discharge capacity of 160–165 mA h g^{-1} (close to the theoretical value of 170 mA h g^{-1}) was observed at low rates. We observed negligible capacity fading: the extent of decay was less than 0.025 mA h g^{-1} per cycle at the 1C rate for over 300 cycles. Excellent cycling behavior was also observed at 60 °C.

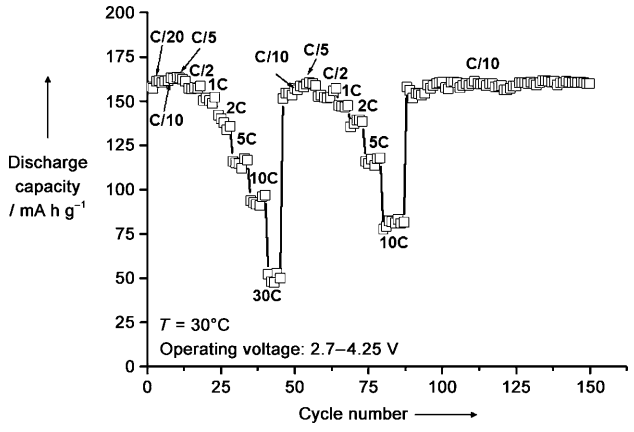

Figure 5. Typical cycling behavior of Li/C–$LiMn_{0.8}Fe_{0.2}PO_4$ coin-type cells at 30 °C with the standard electrolyte solution at various rates of discharge. The rate of discharge was changed repeatedly during the experiment as indicated. A constant current–constant voltage cycling protocol was used with a potentiostatic step at 4.25 V; the constant voltage was applied until the current reached a value corresponding to the C/50 rate.

The new electrode material presented herein was also studied extensively in real lithium-ion cells versus graphite anodes (see Figure S12 in the Supporting Information for representative results). Finally, we studied the thermal behavior of the C–$LiMn_{0.8}Fe_{0.2}PO_4$ cathode material, as this characteristic determines the safety of lithium-ion batteries (thermal stability is critical for EV applications). For comparison, the thermal reactivity of pristine and electrochemically delithiated C–$LiMn_{0.8}Fe_{0.2}PO_4$, C–$LiMnPO_4$ (synthesized for this study) and C–$LiFePO_4$ (commercial product) in $LiPF_6$ (1 M)/EC–DMC (1:1) was measured by differential scanning calorimetry (DSC; see Figure S13 a–c in the Supporting Information for the results (specific heat evolution with respect to temperature)). The thermal stability of pristine C–$LiMn_{0.8}Fe_{0.2}PO_4$ falls between that of C–$LiMnPO_4$ and C–$LiFePO_4$, whereas the thermal stability of delithiated C–$LiMn_{0.8}Fe_{0.2}PO_4$ is higher than that of delithiated C–$LiMnPO_4$ and C–$LiFePO_4$ in terms of both the onset temperatures of the main thermal reactions and the specific heat evolution. Parallel studies[12,13] showed that all $LiMPO_4$ cathode materials examined in this study are much less reactive with standard electrolyte solutions than $Li(MnNiCo)O_2$ and $Li(NiCoAl)O_2$ compounds in terms of both onset temperatures and specific heat evolution.

In conclusion, carbon-coated nanoparticles of $LiMn_{0.8}Fe_{0.2}PO_4$ olivine form a superb cathode material for lithium-ion batteries. This high-capacity cathode material (capacity around 165 mA h g^{-1}) showed very fast rate capabilities and excellent thermal stability. It performed better in terms of these properties than all competing materials based on transition-metal oxides. Of its total capacity, 80 % can be realized in a flat region of the potential profile, at around 4.1 V versus Li/Li^+. Most advanced cathode materials based on transition-metal oxides have a sloping potential profile (4.4–2.5 V). Hence, lithium-ion batteries comprising $LiMn_{0.8}Fe_{0.2}PO_4$ cathodes may reach impressively high energy density.

We attribute the excellent performance of this material to the highly stable lattice structure of the olivine materials and to the fact that their oxygen atoms are much less reactive with standard solution components than those of lithiated transition-metal oxides. Therefore, it is possible to use such materials as nanoparticles and thus to benefit from the fast kinetics of Li insertion into very small, high-surface-area particles, without paying the penalty of high surface reactivity. The carbon coating enables the active mass to have excellent electronic conductivity and also serves as a barrier against detrimental surface reactions between the active mass and solution species.

Although $LiMn_{1-y}Fe_yPO_4$ compounds have been described previously,[9] $LiMn_{0.8}Fe_{0.2}PO_4$ had not been identified as a novel and highly promising practical cathode material until now. Rigorous structural studies will be required to enable a precise explanation of the advantage of the use of a mixture of Mn and Fe ions in the olivine framework. However, we can make several hypotheses on the basis of previous studies (see the Supporting Information for an extended discussion):[6,8,9,14,15] Olivine compounds include single, 1D channels for lithium-ion transport. Hence, any disorder in which transition-metal ions block these channels closes paths for lithium-ion transport. The substitution of Fe ions for some of the Mn ions of $LiMnPO_4$ may contribute to the occurrence of fewer defects in the mixed-transition-metal compound owing to its effect on the synthesis of the material. As a result, both the capacity and the kinetics of the cathode material should be improved relative to those of $LiMnPO_4$. The presence of both Fe and Mn ions in the olivine material may also increase the size of the solid-solution zone of $Li(MnFe)PO_4/(MnFe)PO_4$ relative to that of $LiMnPO_4$ and may thus improve the kinetics of the former compound. Finally, the substitution of Fe ions for some Mn ions may improve the electronic conductivity of the material.

Experimental Section

The C–$LiMn_{0.8}Fe_{0.2}PO_4$ compound with an olivine structure was synthesized by a solid-state reaction between $MnCO_3$ (Aldrich, 99.9%), organoiron(II) compounds, such as $Fe(C_2O_4)_2{\cdot}2H_2O$ (Aldrich, 99%), and LiH_2PO_4 (Aldrich 99%), which were mixed thoroughly with carbon (10 wt%). The mixture was reground by high-energy ball milling and sintered in an argon–hydrogen atmosphere at 550°C for 3 h. $LiFePO_4$ (3% carbon coating) was obtained from Süd-Chemie Inc. $LiMnPO_4$ was prepared as described in Ref. [8]. We used lithium-battery-grade $LiPF_6$ (1M)/EC–DMC (1:1) and $LiPF_6$ (1.5M)/EC–DMC (1:2) electrolyte solutions from UBE Industries Inc. and Tomiyama Inc. (Japan), respectively, as received.

The material was characterized by powder X-ray diffraction, Raman spectroscopy, high-resolution transmission and scanning electron microscopy, Mössbauer, FTIR, and photoelectron spectroscopy, and differential scanning calorimetry (DSC; see the Supporting Information for details of the relevant instrumentation). The particle-size distribution was measured with a Mastersizer-2000 particle-size analyzer (Malvern Instruments Ltd.), the BET surface area was measured with a Micromeritics Gemini 2375 instrument, and the amount of carbon in the C–$LiMn_{0.8}Fe_{0.2}PO_4$ composite was determined by CHN analysis with an EA 1110 elemental analyzer.

For electrochemical measurements, two- and three-electrode coin-type 2325 cells (parts from NRC, Canada) were used with a polypropylene separator from Celgard Inc. The composite working electrode comprised 90.5% C–$LiMn_{0.8}Fe_{0.2}PO_4$, 2% carbon black (i.e. 12.5% total carbon), and 7.5% PVdF binder (all by weight). For the comparative experiments with different cathode materials, we used composite electrodes of similar compositions. Slurries containing these three components in N-methylpyrrolidone were prepared and coated on aluminum-foil current collectors. The electrodes were dried well (vacuum) and pressed (5×10^5 g cm^{-2}) before use. The working electrodes comprised approximately 5 mg of the active mass. A lithium disk and a lithium chip served as the counter and reference electrode, respectively. Electrochemical cells were assembled under an atmosphere of highly pure argon in a glove box. The electrochemical measurements (cyclic voltammetry, impedance spectroscopy, chronopotentiometry) in three-electrode coin-type cells were made with battery test unit model 1470 coupled with FRA model 1255 from Solartron, Inc. Galvanostatic charge–discharge cycling was carried out with a multichannel battery tester from Maccor, Inc. (model 2000) in two-electrode coin-type cells. A constant current–constant voltage (CC–CV) protocol was used with a potential range of 2.7–4.25 V at various rates with potentiostatic steps at the cutoff potential. The constant voltage was applied until the charging current dropped to values corresponding to a C/50 rate.

Aging tests of powders in solution were carried out in polyethylene vials with magnetic stirring under an atmosphere of highly pure argon at 30 and 60°C. The powders were then separated from the solution with a centrifuge, washed several times with pure DMC under an argon atmosphere, and dried under vacuum.

Received: July 1, 2009
Revised: August 25, 2009
Published online: September 30, 2009

Keywords: cathode materials · lithium batteries · nanoparticles · surface chemistry · thermal stability

[1] A. K. Padhi, K. S. Nanjundaswamy, J. B. Goodenough, *J. Electrochem. Soc.* **1997**, *144*, 1188.
[2] S.-Y. Chung, J. T. Bloking, Y.-M. Ching, *Nat. Mater.* **2002**, *1*, 123.
[3] P. P. Prosini, D. Zane, M. Pasquali, *Electrochim. Acta* **2001**, *46*, 3517.
[4] P. Reale, S. Panero, B. Scrosati, J. Garche, M. Wohlfahrt-Mehrens, M. Wachtler, *J. Electrochem. Soc.* **2004**, *151*, A2138.
[5] N. Ravet, A. Abouimrane, M. Armand, *Nat. Mater.* **2003**, *2*, 702.
[6] B. Kang, G. Ceder, *Nature* **2009**, *458*, 190.
[7] Y.-S. Hu, Y.-G. Guo, R. Dominko, M. Gaberscek, J. Jamnik, J. Maier, *Adv. Mater.* **2007**, *19*, 1963.
[8] S. K. Martha, B. Markovsky, J. Grinblat, Y. Gofer, O. Haik, E. Zinigrad, D. Aurbach, T. Drezen, D. Wang, G. Deghenghi, I. Exnar, *J. Electrochem. Soc.* **2009**, *156*, A541.
[9] A. Yamada, Y. Takei, H. Koizumi, N. Sonoyama, R. Kanno, *Chem. Mater.* **2006**, *18*, 804.
[10] A. Yamada, S.-C. Chung, *J. Electrochem. Soc.* **2001**, *148*, A960.
[11] D. Aurbach, B. Markovsky, G. Salitra, E. Markevich, Y. Talyossef, M. Koltypin, L. Nazar, B. Ellis, D. Kovacheva, *J. Power Sources* **2007**, *165*, 491.
[12] O. Haik, S. K. Martha, H. Sclar, Z. Samuk-Fromovich, E. Zinigrad, B. Markovsky, D. Kovacheva, N. Saliyiski, D. Aurbach, *Thermochim. Acta* **2009**, *493*, 96.
[13] S. K. Martha, H. Sclar, Z. Framovich, D. Kovacheva, N. Saliyski, Y. Gofer, P. Sharon, E. Golik, B. Markovsky, D. Aurbach, *J. Power Sources* **2009**, *189*, 248.
[14] C. Delmas, M. Maccario, L. Croguennec, F. L. Cras, F. Weill, *Nat. Mater.* **2008**, *7*, 665.
[15] P. Gibbot, M. Casa-Cabanas, L. Laffont, S. Levasseur, P. Carlach, S. Hamelet, J.-M. Tarascon, C. Masquelier, *Nat. Mater.* **2008**, *7*, 741.

